RSC Advances

PAPER

View Article Online
View Journal | View Issue

Cite this: *RSC Adv.*, 2024, **14**, 2422

Self-assembled nanovesicles based on chiral bis-H_8-BINOL for Fe^{3+} recognition and secondary recognition of L-cysteine by 1 + 1 complex†

Jisheng Tao,[a] Huizhen Wang,[a] Yue Sun,[b] Xiaoxia Sun *[a] and Yu Hu*[b]

Received 9th November 2023
Accepted 8th January 2024

DOI: 10.1039/d3ra07654g

rsc.li/rsc-advances

A novel fluorescent "off" sensor, *R*-β-D-**1**, was obtained in high yield (91.2%) by using octahydronaphthol as a backbone, introducing an alkyne group at the 2-position, and linking azido-glucose *via* a click reaction. The sensor was analyzed by scanning electron microscopy and transmission electron microscopy and was found to be a self-assembled vesicle. AFM results showed that the fluorescence burst was extinguished by the addition of Fe^{3+}, and the fluorescence was restored by the addition of cysteine. This is due to charge transfer within the molecular structure, resulting in the ICT effect and phototransfer of electrons (PET), as well as redshifting (from 331 nm to 351 nm) and quenching of the fluorescence. The self-assembled vesicles of the fluorescent sensor *R*-β-D-**1** encapsulated Fe^{3+}, but upon addition of cysteine, the vesicles of *R*-β-D-**1**–Fe^{3+} were also complexed with it, forming the *R*-β-D-**1**–Fe^{3+}–L-Cys complex, at which point fluorescence gradually returned. Therefore, the fluorescence test of this probe showed that the lowest detection limit of iron ions was 1.67×10^{-7} mol L^{-1}, and its complexation mode was in the form of 1 + 1. The novel probe formed by *R*-β-D-**1**–Fe^{3+} can be used for the fluorescence detection of cysteine.

Introduction

Vesicles are self-assembled nanoparticles that, due to their unique hollow structure, can be used as drug carriers in medical therapies, transporting drug molecules to reach targeted cells and protecting surrounding healthy tissues.[1,2] In this respect, vesicles are similar in structure to cell membranes and can be used to mimic biological membranes, which has attracted the interest of many researchers.[3] The vesicle membrane can be used for molecular recognition through metal ion coordination, hydrogen bonding and other non-covalent bonding effects. In addition, metal coordination-induced vesicle aggregation can help to better understand the role of metal ions in cell membrane movement, as phospholipids in cell membranes are able to form complexes with some specific metal ions, such as Ca^{2+}.[4,5] Selective metal ions can trigger vesicle aggregation through rational building block design. Thus, vesicle aggregation systems may be a good platform for metal ion sensors, which are less often mentioned.

Due to the importance of transition metal ions in biology and the environment, the design and synthesis of fluorescent sensors that can effectively recognize transition metal ions has attracted great interest.[6–10] The pollution by metal ions is increasing today with the rapid development of modern industry, especially industrial effluents discharged into rivers and lakes, *etc.* The pollution caused by transition metal ions pollution is the most serious, of which Fe^{3+} pollution is the most common. If the Fe^{3+} content in fresh water (especially drinking water) is insufficient or excessive, it will cause a series of problems. For example, too much Fe^{3+} in human body will cause iron poisoning and increase the chance of intestinal cancer; too little lead to cause anemia, low immunity and other adverse reactions.[11–15] Excess Fe^{3+} in rivers may lead to the death or overpopulation of aquatic organisms, so rapid detection of the presence of Fe^{3+} is essential.[16] Amino acids have important roles in living organisms, for example, methionine can participate in detoxification reactions in the liver, which can promote the discharge of toxic substances, with certain antioxidant effects; arginine can promote the synthesis of urea in the human body, thus reducing the concentration of blood ammonia, so it is very important to detect arginine, and it is very convenient and fast to detect it by the method of fluorescence sensor[17–19] and cysteine also plays a very important role in the human body such as skin damage, hair discoloration, lethargy and other issues. There are many ways for organisms to ingest cysteine; animals mainly ingest cysteine through feed, while humans mainly ingest cysteine through milk and food.[20–26] Therefore, the detection of cysteine is very important, and the fluorescent probe assay has a great advantage with the

[a]*Jiangxi Key Laboratory of Organic Chemistry, Jiangxi Science and Technology Normal University, Nanchang, 330013, China. E-mail: sunxiaoxia77@126.com*

[b]*College of Chemistry, Nanchang University, Nanchang, China. E-mail: huyu@ncu.edu.cn*

† Electronic supplementary information (ESI) available. See DOI: https://doi.org/10.1039/d3ra07654g

advantages of high sensitivity and simplicity.[27,28] According to research reports, triazole can be used as a corrosion inhibitor for organic copper[29,30] and is a very important metal complex.[31,32] 1,2,3-Triazole has better affinity and easier coordination with metal ions.[33,34]

In this paper, a 2-substituted 1,2,3-triazole-glucose derivative based on octahydronaphthol was synthesized by introducing glucose molecules *via* click reaction. It can be observed by scanning electron microscopy (SEM) that the new fluorescent probe self-assembles in ethanol solution into a vesicular structure suitable for the recognition of Fe^{3+}, which has not been reported in the literature. The fluorescence properties of the derivative were investigated and it was found to selectively recognize Fe^{3+} and to provide secondary recognition of cysteine. The secondary recognition of the sensor *R*-β-D-**1** with Fe^{3+} and cysteine was probed using SEM and TEM.

Experimental

Reagents and instruments

To remove impurities, all solvents were redistilled before use. The analytically pure chemicals used were supplied by pharmaceutical companies or synthesized by routes known in our laboratory. The corresponding metal nitrates or chlorides were used to configure 0.1 M metal ions in methanol solutions. $FeCl_3$ was used as the source of Fe^{3+} unless otherwise noted. TMS was used as the internal standard and chloroform-D or dimethylsulfoxide-D_6 was used as the solvent. ^{13}C NMR and ^{1}H NMR were measured by a Bruker AM-400WB spectrometer. Fluorescence emission spectra were measured by Hitachi F-7100 fluorescence spectrometer unless otherwise stated. Electrospray mass spectra were detected by a Bruker Amazon SL ion trap MS.

R-2,2′-Bis(prop-2-yn-1-yloxy)-5,5′,6,6′,7,7′,8,8′-octahydro-1,1′-binaphthalene (0.20 g, 0.54 mmol) and 1-azido-2,3,4-triacetoxy-5-acetoxymethyl-D-glucose (0.44 g, 1.19 mmol). Under argon protection, 5 mL of tetrahydrofuran was added to the system. The ice bath was stirred for a few minutes to dissolve it completely, next, sodium ascorbate (0.24 g, 1.18 mmol) and anhydrous copper sulfate (0.13 g, 0.54 mmol) were accurately weighed and dissolved in 4 mL of deionized water, shaken well, and when the mixed solution turned to an earthy yellow color, it was added to the reaction system. The system was reacted for 10 h at room temperature and TLC was performed (PE : EA = 4 : 1). The reaction was quenched by adding 10 mL of ice water to the reaction system and the aqueous phase was extracted three times with 30 mL of dichloromethane. The organic phases were then combined, washed once with saturated NaCl solution and dried with anhydrous magnesium sulfate for 30 min. After filtration and rotary evaporation of the solvent, it was separated by column chromatography (PE : EA = 1 : 1). About 0.55 g of white solid was obtained in 91.2% yield. ^{1}H NMR (400 MHz, DMSO-d_6) δ 8.03 (s, 1H), 6.95 (s, 2H), 6.31 (d, J = 8.6 Hz, 1H), 5.59–5.46 (m, 2H), 5.15 (t, J = 9.5 Hz, 1H), 5.05–4.92 (m, 2H), 4.19–3.97 (m, 3H), 2.04–1.96 (m, 8H). ^{13}C NMR (101 MHz, DMSO-d_6) δ 170.06, 169.43, 168.42, 152.95, 144.25, 136.23, 129.61, 128.45, 126.11, 123.10, 111.04, 83.90, 73.49, 72.30, 70.34, 67.73, 61.92, 61.57, 40.36, 39.10, 28.88, 26.79, 22.73, 20.55, 20.35, 19.85.

Results and discussion

According to Scheme 1, the relatively easily synthesized *R*-1 was synthesized from *R*-H_8-BINOL and 3-bromo-1-propyne with moderate yields, respectively. Then the click reactions of *R*-1 and 1-azido-2,3,4-triacetoxy-5-acetoxymethyl-D-glucose were carried out under the catalytic effect of Cu^{+} (formed by the reduction of copper sulfate with sodium ascorbate) to obtain the desired target sensors, respectively. The yields were 89%, respectively. The resulting compounds were structurally characterized by ^{1}H NMR, ^{13}C NMR and ESI-MS.

It was found by DLS that it could self-assemble into vesicles with a tendency to polymerize, and its particle size was about 1–2 μm (Fig. 1). The ability to self-assemble into vesicle structure may be due to the hydrophilicity of the glucose moiety and the hydrophobicity of the benzene ring and triazole moiety.

Fluorescence study

The fluorescence spectral characteristics of the *R*-β-D-**1** fluorescent chemosensor were investigated using a Hitachi F-7100 fluorescence spectrometer. As indicated in Fig. S8,† *R*-β-D-**1** emitted mid-intensity fluorescence at 331 nm (λ_{ex} = 278 nm, EX slit = 2.5 nm, EM slit = 2.5 nm). The effect of *R*-β-D-**1** on different cations (Ba^{2+}, Mn^{2+}, Cu^{+}, Ca^{2+}, K^{+}, Co^{3+}, Cr^{3+}, Zn^{2+}, Al^{3+}, Mg^{2+}, Pb^{2+}, Cu^{2+}, Cd^{2+}, Gd^{3+}, Li^{+}, Na^{+}, NH_4^{+}, Ni^{2+}, and Fe^{3+}) in methanol solution was investigated by fluorescence spectrophotometry. The fluorescence of the sensor *R*-β-D-**1** showed significant fluorescence quenching in response to Fe^{3+}, whereas it did not show significant fluorescence quenching for other ions under the same conditions. Fig. 2 shows the fluorescence of *R*-β-D-**1** and *R*-β-D-**1** with the addition of 5 eq. Fe^{3+}, fluorescence quenching rate of 65%. This indicates that *R*-β-D-**1** is capable of specific fluorescence recognition of Fe^{3+}.

Cations competition studies. In order to further investigate the selectivity and specificity of the fluorescence recognition of Fe^{3+} by *R*-β-D-**1**, we carried out ionic immunity experiments using fluorescence spectrometry on *R*-β-D-**1**, as shown in Fig. S7.† Other 5.0 equivalents of metal ions and the same equivalents of Fe^{3+} were mixed in the assay solution, and the fluorescence response was performed at λ_{ex} = 278 nm and the fluorescence emission intensity was measured. The results of the study showed that the other metal ions had little effect on *R*-β-D-**1**–Fe^{3+}. This suggests that *R*-β-D-**1** can specifically selectively fluoresce in response to Fe^{3+} and can be used as a specific fluorescent probe for detecting background competing ions.

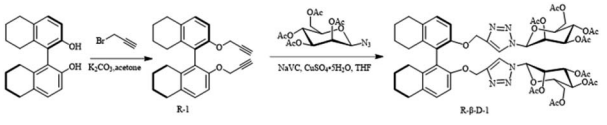

Scheme 1 Synthesis of chiral fluorescence sensor *R*-β-D-**1**.

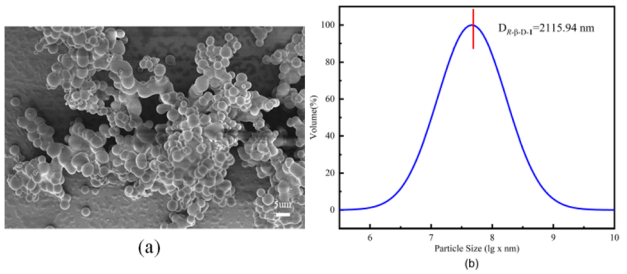

Fig. 1 (a) SEM image of probe *R*-β-D-**1**, (b) DLS assay of probe *R*-β-D-**1** (5 mg mL^{-1} in ethanol).

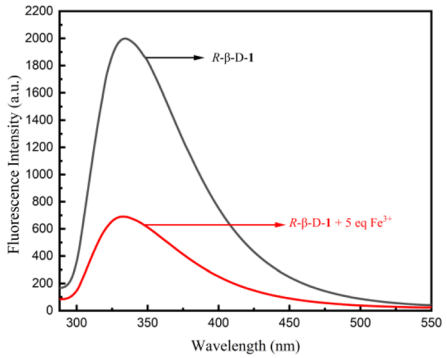

Fig. 2 Fluorescence recognition plot of *R*-β-D-**1** (20 μM, MeOH solution λ_{ex} = 278 nm, EX slit = 2.5 nm, EM slit = 2.5 nm) and Fe^{3+}, the remaining ions are recognized in the ESI.†

The concentration-dependent fluorescence experimental detection of Fe^{3+} by the sensor *R*-β-D-**1** is shown in Fig. 3. According to the results of the titration experiment, as shown in Fig. 3a, the fluorescence intensity of *R*-β-D-**1** at 331 nm gradually decreased and red-shifted to 351 nm when Fe^{3+} increased from 0 to 17 eq. The maximum fluorescence intensity showed a good linear relationship with Fe^{3+} concentration (Fig. 3b).

To determine the complexation of *R*-β-D-**1** with Fe^{3+}, we investigated the bonding affinity of *R*-β-D-**1** with Fe^{3+} and then plotted a Job's plot using the reported method. The total concentration of the mixed solution of *R*-β-D-**1** and Fe^{3+} was kept at 2.0 × 10^{-5} M (R = 0.991) throughout the experiment. Based on the concentration-dependent fluorescence titration experiment (Fig. 4a), the minimum detection limit (LOD) of the novel sensor *R*-β-D-**1** for Fe^{3+} was calculated from "LOD = 3σ/S" as 2.84 × 10^{-7} M. Based on the plots of $I_0/(I_0 - I)$ and 1/[Fe^{3+}], the complexation constant (K_a) of *R*-β-D-**1** with Fe^{3+} was calculated to be 0.33 × 10^4 using the Benesi–Hildebrand equation as shown in Fig. 4b. As shown in the results of Fig. 4c, the molar fraction of [Fe^{3+}] reached a maximum when [Fe^{3+}]/([*R*-β-D-**1**] + [Fe^{3+}]) was about 0.5, indicating that the sensor *R*-β-D-**1** formed a 1 + 1 complex with Fe^{3+}. And based on the fluorescence test data of *R*-β-D-**1**–Fe^{3+} and L-Cys, straight lines of $I/(I_0 - I)$ and 1/[L-Cys] were also fitted for *R*-β-D-**1**–Fe^{3+} and L-Cys. The binding constants of *R*-β-D-**1**–Fe^{3+} and L-Cys, K_a = 4.18 × 10^3 M^{-1}, and the binding affinity, K_d = 2.39 × 10^{-4} M, were calculated as shown in Fig. S10.†

To further demonstrate that the complex *R*-β-D-**1**–Fe^{3+} of the sensor *R*-β-D-**1** with Fe^{3+} was formed in a 1 : 1 stoichiometric ratio, the sensor *R*-β-D-**1** and the complex *R*-β-D-**1**–Fe^{3+} were probed with ESI-MS, and a significant free at m/z = 1139.4050 was obtained, supplied by the [*R*-β-D-**1** + Na^+] *R*-β-D-**1** molecular ion peak (Fig. 5a). Meanwhile, as can be seen from Fig. 6b, the complex *R*-β-D-**1**–Fe^{3+} was trapping an Cl^- and a new peak was found at m/z = 1207.3193 (Fig. 5b). This finding supports our hypothesis that the *R*-β-D-**1**–Fe^{3+} complex has a strong binding affinity for Fe^{3+}.

Fluorescence and absorption titration of amino acids against *R*-β-D-**1**–Fe^{3+}. Fluorescence spectroscopy of the sensor *R*-β-D-**1** was performed using a fluorescence spectrometer to analyze the *R*-β-D-**1**–Fe^{3+} complex as a novel fluorescent sensor for 17 natural amino acids. The fluorescence recognition plots of only *R*-β-D-**1**–Fe^{3+} *versus* L-Cys are presented in Fig. 6a, with the rest of the amino acids recognized in the ESI Fig. S9.† The fluorescence

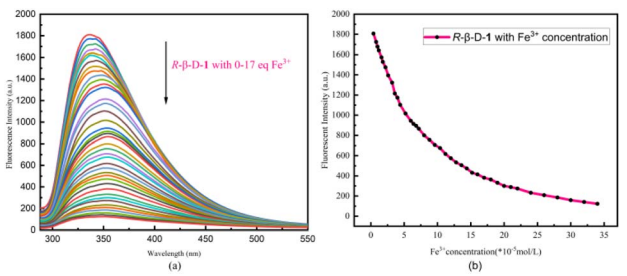

Fig. 3 (a) Fluorescence titration of sensor *R*-β-D-**1** (20 μM in CH_3OH, λ_{ex} = 278 nm, EX slit = 2.5 nm, EM slit = 2.5 nm) with a gradual increase in Fe^{3+} (0.01 M) equivalents (0–17 eq.). (b) Plot of the change in fluorescence intensity of *R*-β-D-**1** at 331 nm with increasing Fe^{3+} concentration.

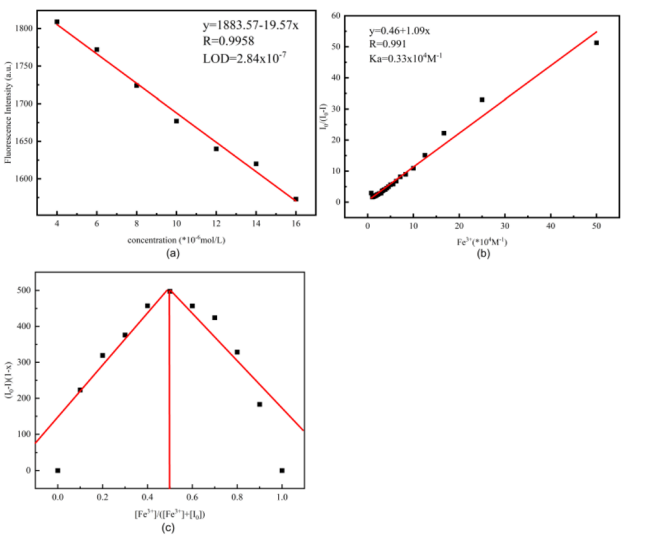

Fig. 4 (a) Linear relationship between fluorescence intensity and Fe^{3+} concentration for *R*-β-D-**1**, calculated for LOD = 2.8 × 10^{-7} M. (b) 1 : 1 combination based on stoichiometric $I_0/(I_0 - I)$ and 1/[Fe^{3+}] Benesi–Hildebrand equation plots. (c) Working curves of 1 : 1 complexes of *R*-β-D-**1** with Fe^{3+}, x is the molar fraction of Fe^{3+}.

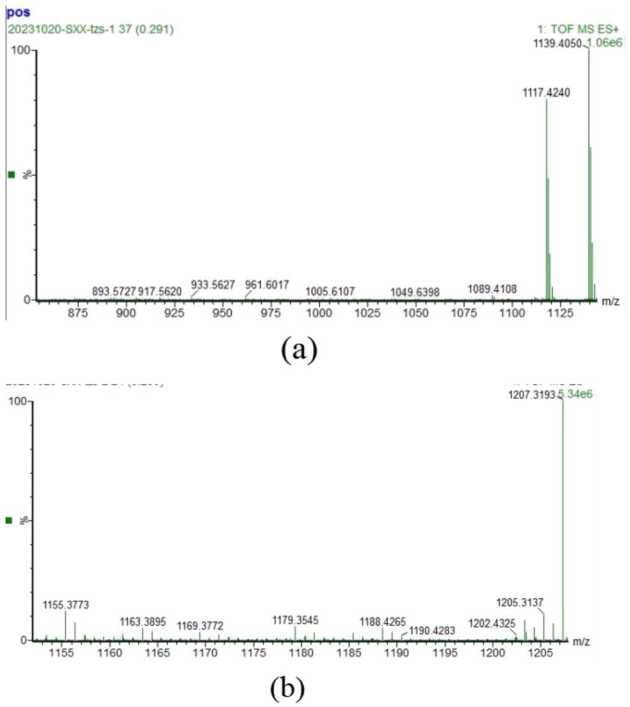

Fig. 5 (a) ESI-MS variation of *R*-β-D-**1**; (b) ESI-MS variation of *R*-β-D-**1**–Fe^{3+}.

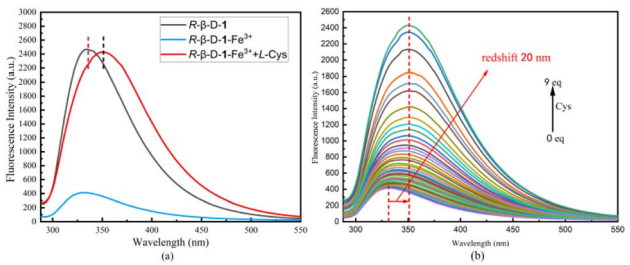

Fig. 6 (a) Is a fluorescence control plot of *R*-β-D-**1**, *R*-β-D-**1** + 10 eq. Fe^{3+}, *R*-β-D-**1** + 10 eq. Fe^{3+} + 10 eq. L-Cys, with the remaining amino acids identified in the ESI.† (b) Fluorescence titration plot of *R*-β-D-**1**–Fe^{3+} (20 μM in MeOH, 10 eq. Fe^{3+}, $\lambda_{ex} = 278$ nm) with gradual increase in Cys (0.01 M) equivalents (0–9 eq.).

selectivity identification experiments were performed by adding 10.0 eq. of different natural amino acids (Phe, His, Lys, Ala, Arg, Ser, Met, Leu, Gly, Val, Asn, Gln, Thr, Glu, Pro, Asp, and Cys) to *R*-β-D-**1**–Fe^{3+} in MeOH solvent. As shown in Fig. 6a, there was some degree of fluorescence enhancement of *R*-β-D-**1**–Fe^{3+} at 331 nm in the presence of Cys, while there were no other significant changes in the fluorescence emission intensity of the other amino acids on the probe. This demonstrated that *R*-β-D-**1**–Fe^{3+} was able to specifically and selectively identify Cys. Meanwhile, fluorescence titration experiments were carried out with Cys against *R*-β-D-**1**–Fe^{3+} as shown in Fig. 6b. During the fluorescence titration of *R*-β-D-**1**–Fe^{3+}, a gradual enhancement of the fluorescence intensity of *R*-β-D-**1**–Fe^{3+} was observed at 331 nm, and the fluorescence intensity reached a maximum with the addition of 9 eq. Cys, with a simultaneous redshift of 20 nm. The titration phenomenon of *R*-β-D-**1** with Cys showed that the fluorescence gradually recovered with the titration of L-Cys, but instead of recovering the original fluorescence of *R*-β-D-**1**, it was red-shifted by 20 nm, which indicated that the L-Cys did not only complex with Fe^{3+}, but rather the three substances, namely, *R*-β-D-**1**, Fe^{3+} as well as L-Cys, complexed, which caused the fluorescence of the sensor to be changed.

Electron microscopy studies. AFM also explored the process of recognition of Fe^{3+} by the sensor *R*-β-D-**1** and secondary recognition of Cys. *R*-β-D-**1** was seen and fluoresced under a microscope when dissolved in ethanol. While fluorescence disappeared from the field of view after the addition of Fe^{3+}, it was restored by the addition of Cys, which was under the same phenomenon as in the fluorescence test (Fig. 7).

R-β-D-**1** was dissolved in ethanol, configured with Fe^{3+} as well as amino acid test solutions, and used for SEM and TEM to obtain Fig. 8a–f. Fig. 8a showed that *R*-β-D-**1** was dispersed vesicles with a particle size of approximately 2 μm. Furthermore, the color of the interior of the vesicles in contrast to the surrounding color suggested that the interior of the vesicles was a hollow structure similar to that of the vesicles formed by phospholipids. After the addition of Fe^{3+}, *R*-β-D-**1**–Fe^{3+} vesicles were obtained, and due to the dynamic properties of the vesicle membrane, the added Fe^{3+} bound to the vesicles, which could be presumed to be due to the vesicles encapsulating the added Fe^{3+} inside the vesicle cavity according to the TEM (Fig. 8e). And after the addition of cysteine, like Fe^{3+}, L-Cys also bound to the sensor *R*-β-D-**1**–Fe^{3+}, forming three compounds of *R*-β-D-**1**–Fe^{3+}–L-Cys complexed together (Fig. 8f). This indicates that the vesicle membrane is soft and flexible. This is the recognition of Fe^{3+} by *R*-β-D-**1** and the secondary recognition of Cys.

Plausible mechanism for sensing of *R*-β-D-1. The plausible sensing mechanism of *R*-β-D-**1**. The article published by our group in 2022 was a monosubstituted xylose structure introduced by click reaction in BINOL,[35] and the fluorescence redshift of its sensor was not obvious after the addition of Fe^{3+}

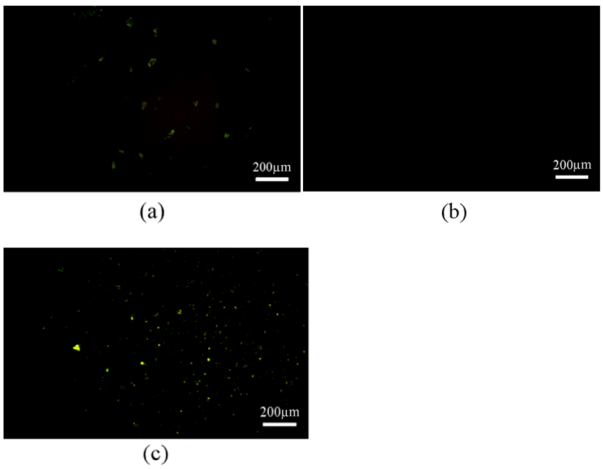

Fig. 7 (a) AFM picture of *R*-β-D-**1** (5 mg mL^{-1} in ethanol), (b) is the AFM picture after addition of Fe^{3+} to *R*-β-D-**1**, (c) is the AFM picture after addition of L-Cys to *R*-β-D-**1**–Fe^{3+}.

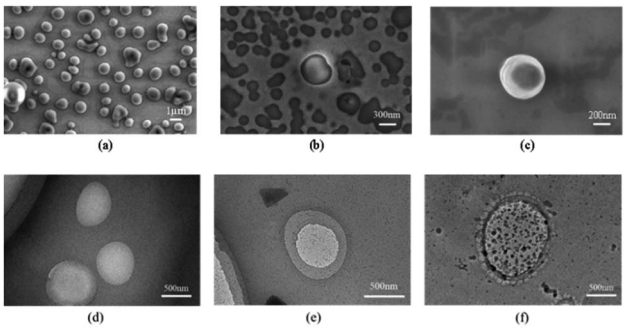

Fig. 8 (a) Is the SEM image of sensor *R*-β-D-**1** (5 mg mL^{-1} in ethanol), (b) is the SEM image of *R*-β-D-**1** with Fe^{3+}, (c) is the SEM image of L-Cys added to *R*-β-D-**1**–Fe^{3+}, (d) is the TEM image of sensor *R*-β-D-**1**, (e) is the TEM image of Fe^{3+} added to sensor *R*-β-D-**1**; (f) is the TEM plot of the addition of L-Cys in *R*-β-D-**1**–Fe^{3+}.

and blueshifted to the initial fluorescence of the sensor after the addition of L-Cys, whereas in this paper, we introduced a double-substituted glucose on H_8-BINOL, and the introduced glycan structures with different spatial resistances were not the same, and a significant redshift occurred after the addition of Fe^{3+} and no blueshift to the initial fluorescence of the sensor after the addition of L-Cys in the case of *R*-β-D-**1**, a significant redshift occurred after the addition of Fe^{3+}, and there was no blue shift to the initial fluorescence after the addition of L-Cys, so the fluorescence phenomenon and mechanism of the two are not the same.

According to the structural analysis of the sensor *R*-β-D-**1**, the rational mechanism for the recognition of Fe^{3+} and the secondary recognition of L-Cys is the intramolecular charge transfer effect (ICT) and phototropic electron transfer (PET),[36,37] this is due to the fact that the N-3 of 1,4-disubstituted triazole can easily act as an electron acceptor,[38–40] and the addition of Fe^{3+} acts as an electron donor, and the coordination between the two is easy to occur, which leads to the red-shift of fluorescence, and the electron jump from the ground state to the excited state of *R*-β-D-**1** induced by light, and the electron in the excited state can not go back to the ground state after the addition of Fe^{3+}, which leads to the quenching of fluorescence. And after the addition of L-Cys, the HS-group in cysteine is easy to coordinate with metal ions,[41] and then combined with fluorescence titration Fig. 6b, fluorescence did not return to the starting fluorescence but redshifted from 331 nm to 351 nm, in addition to then according to the TEM of Fig. 8f also proved the possibility of the three compounds complexed together. In order to further understand the recognition mechanism of *R*-β-D-**1** with Fe^{3+}, we performed DFT calculations. Density functional calculations of B3LYP/6-31G were carried out using the Gaussian 16W program, and the structure of *R*-β-D-**1** before and after coordination with Fe^{3+} was calculated by taking into account the dispersion correction of GD3BJ (Fig. 9). From the figure, it can be found that Fe^{3+} complexes with the 3-N of 1,2,3-triazole, forming Fe^{3+}–N bonds with bond lengths of 2.13 Å and 2.11 Å, which verifies the conjecture of our mechanism.

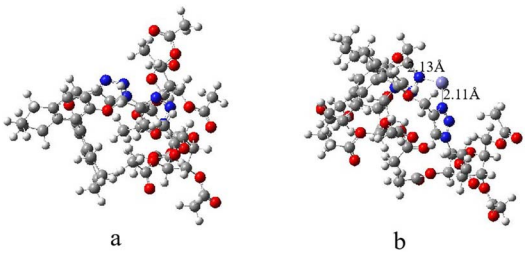

Fig. 9 (a) Shows the structure of the sensor *R*-β-D-**1** and (b) shows the structure of the *R*-β-D-**1**–Fe^{3+} coordination.

Conclusions

H_8-BINOL–glucose derivatives were synthesized and characterized from azido glucose and *R*-H_8-BINOL. The fluorescence properties of metals were investigated by spectroscopic techniques. The high selectivity and sensitivity of the sensor *R*-β-D-**1** in Fe^{3+} sensing was confirmed by fluorescence response experiments, competition experiments and fluorescence titration experiments on 19 different metal ions. The stoichiometry and coordination of the complexes were determined by ESI-MS and fluorescence emission spectroscopy, confirming the existence of 1 + 1 mode binding between the sensor *R*-β-D-**1** and Fe^{3+}. The fluorescence response of the *R*-β-D-**1**–Fe^{3+} complex to amino acids was further explored using the *R*-β-D-**1**–Fe^{3+} complex as a novel fluorescent probe, and it was found that *R*-β-D-**1**–Fe^{3+} could perform secondary recognition of Cys. *R*-β-D-**1**–Fe^{3+} produced selective fluorescence enhancement of Cys in 17 natural amino acids through the interactions of the –SH side chain, which enabled *R*-β-D-**1** and *R*-β-D-**1**–Fe^{3+} complex systems more attractive. In addition, SEM and TEM were also used to study the process of *R*-β-D-**1** and Fe^{3+} and secondary recognition of L-Cys. It was found that after the sensor *R*-β-D-**1** complexed with Fe^{3+}, L-Cys was added to make the sensor vesicle wrap it together. These three compounds, *R*-β-D-**1**–Fe^{3+}–L-Cys, were complexed together. The results suggest that *R*-β-D-**1** can be used as a specific fluorescent probe for the detection of Fe^{3+} and can help to recognize Cys.

Conflicts of interest

There are no conflicts to declare.

Acknowledgements

The authors are grateful for the financial support of the National Natural Science Foundation of China (No. 21462018 and 21861025), the Science Fund of the Technology Office of Jiangxi, China (20192BAB203003) and University-Industry Collaborative Education Program (202102249008).

Notes and references

1 L. Wang, G. Wang, W. Mao, Y. Chen, M. M. Rahman, C. Zhu, P. M. Prisinzano, B. Kong, J. Wang, L. P. Lee and Y. Wan,

Bioinspired engineering of fusogen and targeting moiety equipped nanovesicles, *Nat. Commun.*, 2023, **14**, 3366.
2 J. M. Carnino, Z. Hao Kwok and Y. Jin, Extracellular Vesicles: A Novel Opportunity for Precision Medicine in Respiratory Diseases, *Front. Med.*, 2021, **8**, 661679.
3 J. R. Sanborn, X. Chen, Y. Yao, J. A. Hammons, R. H. Tunuguntla, Y. Zhang, C. C. Newcomb, J. A. Soltis, J. J. De Yoreo, A. Van Buuren, A. N. Parikh and A. Noy, Carbon Nanotube Porins in Amphiphilic Block Copolymers as Fully Synthetic Mimics of Biological Membranes, *Adv. Mater.*, 2018, **30**, 1803355.
4 S. K. De, N. Kanwa and A. Chakraborty, Influence of Trivalent Metal Ions on Lipid Vesicles: Gelation and Fusion Phenomena, *Langmuir*, 2019, **35**, 6429–6440.
5 P. Xing, Y. Wang, M. Yang, Y. Zhang, B. Wang and A. Hao, *ACS Appl. Mater. Interfaces*, 2016, **8**, 17676–17684.
6 A. Nayal, P. K. Muwal and P. S. Pandey, Bile acid based receptors for multiple metal ion recognition, *Tetrahedron*, 2019, **75**, 1968–1974.
7 M. Shi, C. Fu, J. Yu, Y. Yang and P. Shi, A novel 2D metal–organic framework probe: a highly sensitive and visual fluorescent sensor for Al^{3+}, Cr^{3+} and Fe^{3+} ions, *New J. Chem.*, 2022, **46**, 18911–18916.
8 D. Wu, L. Chen, W. Lee, G. Ko, J. Yin and J. Yoon, Recent progress in the development of organic dye based near-infrared fluorescence probes for metal ions, *Coord. Chem. Rev.*, 2018, **354**, 74–97.
9 C. Fu, X. Sun, G. Zhang, P. Shi and P. Cui, Porphyrin-Based Metal–Organic Framework Probe: Highly Selective and Sensitive Fluorescent Turn-On Sensor for M^{3+} (Al^{3+}, Cr^{3+}, and Fe^{3+}) Ions, *Inorg. Chem.*, 2021, **60**, 1116–1123.
10 J.-X. Hou, J.-P. Gao, J. Liu, X. Jing, L.-J. Li and J.-L. Du, Highly selective and sensitive detection of Pb^{2+} and UO_2^{2+} ions based on a carboxyl-functionalized Zn(II)-MOF platform, *Dyes Pigm.*, 2019, **160**, 159–164.
11 X. Liang, X. Li, Y. Tang, L. Hong, W. Wei and X. Liu, Hyperbranched poly(ester ether)s as an amplified fluorescence sensor for selective and sensitive Fe^{3+} detection and bioimaging, *J. Appl. Polym. Sci.*, 2022, **139**, 51865.
12 N. Roy, A. Dutta, P. Mondal, P. C. Paul and T. S. Singh, A new coumarin based dual functional chemosensor for colorimetric detection of Fe^{3+} and fluorescence turn-on response of Zn^{2+}, *Sens. Actuators, B*, 2016, **236**, 719–731.
13 Y. Ma and X. Cheng, Readily soluble cellulose-based fluorescent probes for the detection and removal of Fe^{3+} ion, *Int. J. Biol. Macromol.*, 2023, **253**, 127393.
14 X. Bao, X. Cao, X. Nie, Y. Xu, W. Guo, B. Zhou, L. Zhang, H. Liao and T. Pang, A new selective fluorescent chemical sensor for Fe^{3+} based on rhodamine B and a 1,4,7,10-tetraoxa-13-azacyclopentadecane conjugate and its imaging in living cells, *Sens. Actuators, B*, 2015, **208**, 54–66.
15 Y. Yang, C.-Y. Gao, N. Zhang and D. Dong, Tetraphenylethene functionalized rhodamine chemosensor for Fe^{3+} and Cu^{2+} ions in aqueous media, *Sens. Actuators, B*, 2016, **222**, 741–746.
16 S. Munusamy and S. Kulathu Iyer, A chiral (S)-BINOL based fluorescent sensor for the recognition of Fe(III) and cascade discrimination of α-amino acids, *Tetrahedron: Asymmetry*, 2016, **27**, 492–497.
17 X. Yu, B. Zhang, C. Fan, Q. Yan, S. Wang, H. Hu, Q. Dong, G. Du, Y. Gao and C. Zeng, Rapid, enantioselective and colorimetric detection of D-arginine, *iScience*, 2022, **25**, 104964.
18 X. Yu, B. Zhang, P. Liao, J. Huang, C. Fan, H. Hu, Q. Dong, G. Du, Y. Gao and C. Zeng, A chemoselective fluorescent probe for arginine in aqueous phase, *Dyes Pigm.*, 2022, **203**, 110339.
19 P. Liao, X. Yu, C. Fan, B. Zhang, J. Huang, Y. Wu, G. Du, Q. Dong and C. Zeng, Acrylate-guided chemoselective fluorescent detection of arginine and lysine in aqueous media, *Dyes Pigm.*, 2023, **215**, 111288.
20 C. A. Huerta-Aguilar, B. Ramírez-Guzmán, P. Thangarasu, J. Narayanan and N. Singh, Simultaneous recognition of cysteine and cytosine using thiophene-based organic nanoparticles decorated with Au NPs and bio-imaging of cells, *Photochem. Photobiol. Sci.*, 2019, **18**, 1761–1772.
21 C. A. Huerta-Aguilar, P. Thangarasu and J. G. Mora, Tetraphenylethene functionalized rhodamine chemosensor for Fe^{3+} and Cu^{2+} ions in aqueous media, *J. Mol. Struct.*, 2018, **1157**, 660–671.
22 X. Li, K. Fan, W. Kang, R. Yang, B. Qu and L. Lu, γ-Aminobutyric acid-modified graphene oxide as a highly selective and low-toxic fluorescent nanoprobe for relay recognition of copper(II) and cysteine, *Microchim. Acta*, 2019, **186**, 461.
23 A. K. Shoveller, J. G. Pezzali, J. D. House, R. F. Bertolo, P. B. Pencharz and R. O. Ball, Methionine and cysteine oxidation are regulated in a dose dependent manner by dietary Cys intake in neonatal piglets receiving enteral nutrition, *PLoS One*, 2022, **17**, e0275760.
24 X. Han, Z. Zhai, X. Yang, D. Zhang, J. Tang, J. Zhu, X. Zhu and Y. Ye, A FRET-based ratiometric fluorescent probe to detect cysteine metabolism in mitochondria, *Org. Biomol. Chem.*, 2020, **18**, 1487–1492.
25 T. Song, W. Qin, Z. Lai, H. Li, D. Li, B. Wang, W. Deng, T. Wang, L. Wang and R. Huang, Dietary cysteine drives body fat loss via FMRFamide signaling in Drosophila and mouse, *Cell Res.*, 2023, **33**, 434–447.
26 A. T. S. Wyse, L. D. Bobermin, T. M. Dos Santos and A. Quincozes-Santos, Homocysteine and Gliotoxicity, *Neurotoxic. Res.*, 2021, **39**, 966–974.
27 E. Mirsadoughi, F. Nemati, F. Oroojalian and M. Hosseini, Turn –on FRET-based cysteine sensor by sulfur-doped carbon dots and Au nanoparticles decorated WS_2 nanosheet, *Spectrochim. Acta, Part A*, 2022, **272**, 120903.
28 R. Jia, K. Jin, J. Zhang, X. Zheng, S. Wang and J. Zhang, Colorimetric and fluorescent detection of glutathione over cysteine and homocysteine with red-emitting N-doped carbon dots, *Sens. Actuators, B*, 2020, **321**, 128506.
29 V. S. Bieber, E. Ozcelik, H. J. Cox, C. J. Ottley, J. K. Ratan, M. Karaman, M. Tabakci, S. K. Beaumont and J. P. S. Badyal, Capture and Release Recyclable

Dimethylaminomethyl-Calixarene Functional Cloths for Point-of-Use Removal of Highly Toxic Chromium Water Pollutants, *ACS Appl. Mater. Interfaces*, 2020, **12**, 52136–52145.

30 J.-L. Chen, X.-H. Zeng, P. Ganesan, L.-H. He, J.-S. Liao, S.-J. Liu, H.-R. Wen, F. Zhao and Y. Chi, Heterobimetallic Copper(i) Complexes Bearing Both 1,1′-Bis(Diphenylphosphino)Ferrocene and Functionalized 3-(2′-Pyridyl)-1,2,4-Triazole, *New J. Chem.*, 2019, **43**, 4261–4271.

31 M. Simmons, K. Cummings Premack, E. D. Guerra, M. J. Bohle, K. A. Rosadiuk and D. S. Bohle, 2,3,5-Metallotriazoles: Amphoteric Mesoionic Chelates from Nitrosoguanidines, *Inorg. Chem.*, 2021, **60**, 9621–9630.

32 G. Singh, Diksha, A. Singh, P. Satija, Pawan, Mohit, D. González-Silvera, C. Espinosa-Ruíz and M. A. Esteban, Organosilanes and Their Magnetic Nanoparticles as Naked Eye Red Emissive Sensors for Ag^{+} Ions and Potent Anti-Oxidants, *New J. Chem.*, 2021, **45**, 5517–5525.

33 S. U. Ofoegbu, T. L. P. Galvão, J. R. B. Gomes, J. Tedim, H. I. S. Nogueira, M. G. S. Ferreira and M. L. Zheludkevich, Corrosion inhibition of copper in aqueous chloride solution by 1H-1,2,3-triazole and 1,2,4-triazole and their combinations: electrochemical, Raman and theoretical studies, *Phys. Chem. Chem. Phys.*, 2017, **19**, 6113–6129.

34 R. Balasubramanian, M. I. Fathima Rigana, P. Thirukumaran, R. Atchudan, M. Sarojadevi and J. Lee, Synthesis and properties of polytriazoleimide containing anthracene, pyridine and 1,2,3-triazole groups and their nanocomposites with titanium dioxide, *Polym. Eng. Sci.*, 2019, **59**, 129–138.

35 H. Wang, Y. Liu, Y. Zhang and X. Sun, Synthesis of BINOL–Xylose-Conjugates as "Turn-off" Fluorescent Receptors for Fe^{3+} and Secondary Recognition of Cysteine by Their Complexes, *RSC Adv.*, 2022, **12**, 10379–10385.

36 K. Xiong, F. Huo, J. Chao, Y. Zhang and C. Yin, Colorimetric and NIR Fluorescence Probe with Multiple Binding Sites for Distinguishing Detection of Cys/Hcy and GSH In Vivo, *Anal. Chem.*, 2019, **91**, 1472–1478.

37 B. Karasulu and W. Thiel, Photoinduced Intramolecular Charge Transfer in an Electronically Modified Flavin Derivative: Roseoflavin, *J. Phys. Chem. B*, 2015, **119**, 928–943.

38 V. K. Tiwari, B. B. Mishra, K. B. Mishra, N. Mishra, A. S. Singh and X. Chen, Cu-Catalyzed Click Reaction in Carbohydrate Chemistry, *Chem. Rev.*, 2016, **116**, 3086–3240.

39 D. S. Pedersen and A. Abell, 1,2,3-Triazoles in Peptidomimetic Chemistry, *Eur. J. Org Chem.*, 2011, 2399–2411.

40 A. K. Agrahari, P. Bose, M. K. Jaiswal, S. Rajkhowa, A. S. Singh, S. Hotha, N. Mishra and V. K. Tiwari, Cu(I)-Catalyzed Click Chemistry in Glycoscience and Their Diverse Applications, *Chem. Rev.*, 2021, **121**, 7638–7956.

41 M. Lu, Y. Duan, Y. Song, J. Tan and L. Zhou, Green preparation of versatile nitrogen-doped carbon quantum dots from watermelon juice for cell imaging, detection of Fe^{3+} ions and cysteine, and optical thermometry, *J. Mol. Liq.*, 2018, **269**, 766–774.